HHS Public Access

Author manuscript

Curr Biol. Author manuscript; available in PMC 2022 February 08.

Published in final edited form as:

Curr Biol. 2021 February 08; 31(3): 635–642.e3. doi:10.1016/j.cub.2020.10.091.

Theta but not gamma oscillations in area V4 depend on input from primary visual cortex

Ricardo Kienitz[1,2,3,10], **Michele A Cox**[4,5], **Kacie Dougherty**[4,6], **Richard C Saunders**[7], **Joscha T Schmiedt**[1], **David A Leopold**[7,8], **Alexander Maier**[4], **Michael C Schmid**[2,9]

[1]Ernst Strüngmann Institute (ESI) for Neuroscience in Cooperation with Max Planck Society, Deutschordenstraße 46, 60528 Frankfurt a. M., Germany [2]Institute of Neuroscience, Newcastle University, Framlington Place, Newcastle upon Tyne NE2 4HH, UK [3]Epilepsy Center Frankfurt Rhine-Main, Center of Neurology and Neurosurgery, Goethe University, Schleusenweg 2-16, 60528 Frankfurt a.M., Germany [4]Department of Psychology, Vanderbilt University, 111 21st Avenue South, 301 Wilson Hall, Nashville, TN 37240, USA [5]Department of Brain and Cognitive Sciences - University of Rochester, Meliora Hall, University of Rochester, Rochester, NY 14627 [6]Princeton Neuroscience Institute, Princeton University, Washington Rd, Princeton, New Jersey 08544, USA [7]Laboratory of Neuropsychology, NIMH, Convent Drive 49, Bethesda, MD 20892, USA [8]Neurophysiology Imaging Facility, NIMH, NINDS & NEI, 49 Convent Drive, Bethesda, MD 20892, USA [9]Faculty of Science and Medicine, Chemin du Musée 5, 1700 Fribourg, Switzerland [10]Lead Contact

Summary

Theta (3–9 Hz) and gamma (30–100 Hz) oscillations have been observed at different levels along the hierarchy of cortical areas and across a wide set of cognitive tasks. In the visual system, the emergence of both rhythms in primary visual cortex (V1) and mid-level cortical areas V4 have been linked with variations in perceptual reaction times [1–5]. Based on analytical methods to infer causality in neural activation patterns, it was concluded that gamma and theta oscillations might both reflect feedforward sensory processing from V1 to V4 [6–10]. Here we report on experiments in macaque monkeys in which we experimentally assessed the presence of both oscillations in the neural activity recorded from multi-electrode arrays in V1 and V4 before and after a permanent V1-lesion. With intact cortex theta and gamma oscillations could be reliably elicited in V1 and V4 when monkeys viewed a visual contour illusion and showed phase-to-amplitude coupling. Laminar analysis in V1 revealed that both theta and gamma oscillations

Correspondence: michael.schmid@unifr.ch or ricardo.kienitz@esi-frankfurt.de.

Author contributions

Conceptualization A.M., D.A.L., M.C.S.; Methodology, A.M., D.A.L., R.C.S., M.C.S..; Software, A.M., D.A.L., M.A.C., K.D., R.K., J.T.S, M.C.S.; Formal Analysis, R.K.; Investigation, A.M., D.A.L., R.C.S., R.K., M.A.C, K.D., M.C.S.; Writing – Original Draft, R.K. and M.C.S.; Writing – Review & Editing, all authors; Supervision, M.C.S.; Funding Acquisition, A.M., D.A.L., M.C.S.

Declarations of Interest

The authors declare no competing financial interests.

occurred primarily in the supragranular layers, the cortical output compartment of V1. However, there was a clear dissociation between the two rhythms in V4 that became apparent when the major feedforward input to V4 was removed by lesioning V1: While V1 lesioning eliminated V4 theta, it had little effect on V4 gamma power except for delaying its emergence by >100 ms. These findings suggest that theta is more tightly associated with feedforward processing than gamma and pose limits on the proposed role of gamma as a feedforward mechanism.

eTOC Blurb

Kienitz et al. show that upon visual stimulation V1 and V4 show theta and gamma oscillations which interacted in terms of phase-to-amplitude coupling. Lesion of V1, the major input source to V4, eliminated V4 theta oscillations. In contrast V4 gamma oscillations were less affected, still contained stimulus information but emerged delayed (>100 ms).

Keywords

Visual cortex; primary visual cortex (V1); V4; oscillations; rhythms; theta; gamma; lesion; feedforward; feedback

RESULTS

Visual stimulation elicits theta and gamma activity in V1 and V4

To assess theta and gamma oscillations across two different levels of the cortical hierarchy, we recorded multi-unit activity (MUA) and local field potential (LFP) in visual areas V1 and V4 in monkeys that passively viewed a visual contour (‘Kanizsa’) illusion and its non-illusory control (Figure 1 A). This visual stimulation elicited robust increases in multi-unit activity (MUA) both in V1 and V4, whereas stimulus-specific effects across channels were only seen in V4 (Figure 1B–C, Figure S1A, Table S1, see also Figure 4E–F, left panels, left wings). In addition to this increase in firing rates after stimulus onset, spectral analyses of MUA responses focusing on the sustained response period after stimulus onset (0.3–1s) revealed significant theta oscillations both in V1 and V4 and gamma oscillations in V1 (Figure 1B–C, Figure S1A, see Table S2 for detailed statistics). In contrast to the non-rhythmic MUA in V1, both the theta and gamma modulation of V1 MUA showed significantly stronger increases for the illusion compared to the control (Figure 1B, Table S2). Similarly, V4 exhibited strong theta oscillations associated with the Kanizsa illusion (Figure 1C, see also Figure 4E, right panel, left wing and F, right panel, left wing, Table S2).

Analysis of V1 LFP revealed that all channels showed theta and gamma power increases following visual stimulation. However, in contrast to the rhythmic MUA, these power changes were not significantly modulated by the presence of the illusion (Figure 1D, Figure S1B, Table S3, theta: p=0.99, gamma: p=0.97, n=61, Wilcoxon rank sum test). V4 LFP exhibited similar theta oscillations as V4 MUA. Yet, compared to V4 MUA it also showed significant power increases in the gamma range (Figure 1E, Figure S1C–D, Table S3, see also Figure 4G, left and right panel, left wings). Both the theta and gamma activity in V4 proved sensitive to the illusion (see also Figure 4H, left and right panel, left wings). As spiking and gamma oscillations can sometimes be linked to each other [11,12], we

correlated MUA and LFP gamma power and found close to zero correlations between MUA and LFP gamma power across trials in both monkeys (average r = 0.01, n = 60 in monkey B and average r = 0.02, n = 57 in monkey F). No channel showed significant correlations after correcting for multiple comparisons.

In addition to their mere presence in both areas, LFP theta and gamma oscillations showed interactions in time (Figure 2A). Such phase-to-amplitude coupling (PAC) has been proposed as a link between large-scale and local neuronal computation [13] and has been shown to *decrease* with attention-related modulation in electrocorticogram (ECoG) recordings of V1 and V4 [7]. To examine this PAC further in our data, we computed a modulation index (MI) [14] in V1 and V4 (STAR Methods). We found that both V1 and V4 showed significant phase-to-amplitude coupling in the majority of channels, whereas illusion-related modulation was stronger in V4 (Figure 2 B–C, see Table S4 for detailed statistics).

Taken together, visual stimulation elicited theta- and gamma-rhythmic MUA in V1 and theta-rhythmic MUA in V4, all of which carried information about stimulus identity. In the LFP, theta and gamma oscillations were present both in V1 and V4. However, stimulus-specific modulation of rhythmic LFP was more prominent in V4. In addition, gamma amplitude was modulated by theta phase, with stronger illusion-specific effects in V4 and close to no illusion-effects in V1.

Theta and gamma activity predominantly emerge in V1 supragranular layers

Having verified the presence of both theta and gamma rhythms in V1 and V4, our next aim was to assess whether their laminar cortical distribution within V1 as recorded by linear multi-contact electrodes (monkey Br, STAR Methods) is consistent with their proposed role in feedforward processing. While feedforward projections tend to originate from supragranular layers, feedback connections preferentially target extragranular layers [15,16]. Using the laminar designation from the current source density (CSD) profile in response to visual stimulation to identify cortical layers [17] (Figure 3A, STAR Methods), we analyzed the theta-MUA as well as theta and gamma LFP as a function of V1's cortical depth (Figure 3B). This revealed that peak MUA theta power is specific to the superficial layers. For theta-range LFP, an additional peak emerged in V1's infragranular layers. Gamma-range power of the LFP peaked (supra-)granularly, in line with previous findings [18]. In summary, the predominant supragranular localization of theta and gamma oscillations supports the proposed engagement of both rhythms in feedforward processing, as V1 projections to V4 originate in supragranular layers [15,16].

V1 lesion diminishes spiking and eliminates theta activity in V4

Our next aim was to experimentally test the proposed feedforward hypothesis of theta and gamma oscillations, by longitudinally comparing V4 activity before and after a focal V1 lesion that causes persistent cortical blindness [19,20] and removes the major feedforward sensory input source to V4. Stimulus-specific changes were assessed by a sensitivity measure d' where positive values indicate stronger responses to the illusionary stimulus compared to the control (STAR Methods). We first examined non-rhythmic components of

the recorded signals. Although lesioning V1 removed the largest part of V4 activity (Figure 4A), residual visually evoked MUA responses were still significantly present in almost all electrodes ($p<0.05$, Wilcoxon signed rank test, Figure 4E, left panel), likely due to residual input from the V1 lesion boundary or V1-bypassing geniculate input to V4 [19,21–23]. Analysis of MUA onset latencies after the lesion showed a slight delay relative to prelesion conditions of 13.0±2 ms in monkey B ($p=1.9\times10^{-10}$, n = 59) and 7.7±0.5 ms in monkey F ($p=3.8\times10^{-4}$, n = 54). However, the stimulus-selectivity related to the visual illusion was greatly diminished in monkey B or even lost in monkey F after the lesion (d' of Kanizsa-modulated channels, p(pre>post): $p=1\times10^{-6}$, n=37 in monkey B, $p=2\times10^{-5}$, n=24 in monkey F, Wilcoxon signed rank test, Figure 4F, left panel). The stimulus-selectivity related to the visual illusion was thus virtually lost after the V1 lesion. We then used spectral analysis to assess the rhythmic nature of the recorded signals. We first describe the results for theta and in the following section for gamma, as the results differed dramatically for these two rhythms.

Following the V1 lesion, V4 theta rhythmicity disappeared, both for MUA and LFP (see Figure 4B–C, Figure S2A, see Table S5 for further statistics). This loss of theta activity was seen throughout our sampled population. The average theta power for the MUA channels that were visually responsive in the theta range dropped from an average of 167±21% in monkey B and 79±16% in monkey F to the non-significant noise level with residual values of 24±12% and 33±9%, in monkeys B and F, respectively (Figure 4E, right panel, Table S5). Not surprisingly, the corresponding Kanizsa MUA theta d' values dropped from 0.37±0.03 and 0.27±0.02 to non-significant values close to zero in monkey B and F, respectively (Figure 4F, right panel, Table S5).

Analysis of LFP theta oscillations paralleled observations in the MUA domain. The prominent peak in the theta range and its modulation by the illusion stimulus given intact V1 (Figure 1E, 4C) virtually disappeared after the lesion (Figure 4C, 4G–H, left panel, Table S5, SNR>0: $p=0.46$, n=60 in monkey B, $p=0.99$, n=50 in monkey F, Wilcoxon signed rank test). Similarly, LFP-derived theta d' values (Figure 4H, left panel) were no longer significantly positive once V1 was removed ($p=0.28$, n=59 in monkey B, $p=0.99$, n=27 in monkey F, Wilcoxon signed rank test). Thus, although non-rhythmic residual visual activation was present in both monkeys, the neural theta rhythm and its illusion related modulation completely vanished, when V1 input was removed.

V4 gamma oscillations survive V1 lesion

The observed dependence of V4 theta rhythms on V1 input, did not hold for LFP gamma, for which lesioning V1 appeared to have little effect. In fact, visually elicited activity in the low gamma band remained clearly present, despite the severed V1 input (Figure 4C–D, Figure S2B). V4 LFP gamma power responses, averaged across trial-time (Figure 4G, right panel), decreased after the V1 lesion (−16.0±5.13%, n=60, in monkey B and −31.9±2.22%, n=57 in monkey F), but remained overall positive (SNR>0: $p=3.9\times10^{-11}$, n=60 in monkey B, $p=0.001$, n=57 in monkey F, Wilcoxon signed rank test). Even more surprisingly, gamma power was still significantly modulated by the Kanizsa illusion compared to its control condition (d'>0: $p=7.4\times10^{-7}$, n=36 in monkey B and $p=1.9\times10^{-7}$, n=47 in monkey F,

Wilcoxon signed rank test) (Figure 4H, right panel). We performed again a correlation between post-lesion LFP gamma power and residual MUA across trials per channel and found only very weak correlation in both monkeys (r=0.04, n=60 in monkey B and r=0.02, n=57 in monkey F). Only 5 channels in monkey B and 0 channels in monkey F showed significant correlations across trials (Student's t-test, corrected for multiple comparisons). Thus in our data there seemed to be very little relation between V4 MUA and LFP gamma oscillations. This pattern was present under intact conditions and did not change when V1 was lesioned.

Interestingly however, the onset of gamma activity in V4 post-lesion increased by >100 ms compared to pre-lesion conditions (Figure 4D, Figure S2B). On average, following the V1 lesion, gamma power responses significantly exceeded pre-stimulus baseline levels 161.12±31.04ms and 121.01±43.69ms after they did so with intact V1 in monkey B (p=5.2×10^{-6}, n=50, Wilcoxon signed rank test) and F (p=0.0058, n=31, Wilcoxon signed rank test), respectively (Figure 4I, see Figure S2C for absolute latencies). This marked delay by >100 ms in gamma oscillation onset is in contrast with the finding for MUA, for which the onset latency increased by <15 ms post-lesion. Further analysis of the gamma onset latency as function of recording sessions after the V1 lesion showed that significant gamma power was present in each recording session and that there was no consistent effect regarding changes over time across monkeys (which might have been due to postlesional plasticity, Figure S2E).

In addition, we found a decrease in peak gamma frequency without V1 in one monkey (Figure S2B). Specifically, gamma peak frequencies changed on average by −5.73±0.86 Hz in monkey B (p=1.29×10^{-6}, n=49, Wilcoxon signed rank test) and 0.51±0.64 Hz in monkey F (p=0.51, n=60, Wilcoxon signed rank test), respectively, compared to pre-lesion conditions (Figure 4J, see Figure S2D for absolute frequencies).

In summary, while residual MUA responses could still be visually elicited in V4 following V1 lesions, theta activity and Kanizsa-associated modulations of spiking activity were lost. In contrast, gamma activity was well preserved and even contained stimulus-related information that emerged with a significant time-delay compared to pre-lesion conditions.

Discussion

Theta rhythms across the cortical hierarchy

In primates, spiking and LFP theta oscillations have been observed in various cortical as well as subcortical structures during a variety of cognitive tasks [24–35]. Our results show that theta oscillations are present in the spiking of neurons both in V4 and V1. However, whether theta emerges across these cortical areas (like V1 and V4) in parallel via independent local processes [2] or whether it is coordinated to enhance long-range inter-areal communication [32,36,37] remains to be solved. In our data, theta organized gamma oscillations [38] and might be a candidate mechanism for long-distance integration or transfer of information to high-level association areas [32,39,40].

The predominant supragranular occurrence of MUA theta in V1 is in line with it being a feedforward signal [15,16,41] given that supragranular layers project to downstream visual areas. In addition, we found an infragranular peak of LFP theta oscillations. This finding might reflect the LFP's sensitivity to synaptic signals [42,43], in principle arising from either local or remote sources [15,16,41], and therefore does not contradict the feedforward hypothesis of theta. The infragranular LFP theta peak could point towards an integrative role of theta oscillations: While the supragranular MUA theta arguably reflects oscillatory spiking of feedforward projection units, infragranular LFP theta oscillations could reflect local postsynaptic oscillations which might serve to integrate incoming feedback signals to the local computations (e.g. via PAC to gamma oscillations) or to the theta-rhythmic feedforward output. In that sense theta might also help to integrate feedback signals.

In a direct test of the hypothesis that theta spiking represents a feedforward signal [6] by lesioning V1 and recording from V4, our data provide first causal evidence that this may indeed be the case. A theta rhythm that emerges first in early visual cortex and is then transmitted into higher cognitive and motor areas appears as an attractive mechanism for long-range coordination of local activity. This could help explain the wide-spread observations of theta oscillations across a wide set of visuo-motor tasks in various areas, including attentive sampling, saccadic exploration and motor tracking [3,26,27,44–46]. A loss of theta oscillations and stimulus-related information in spiking, as seen here under conditions of cortical blindness from V1 injury, might be indicative of a disrupted cortical information transfer and neurological dysfunction.

Unlikely role of gamma as feedforward signal

Perhaps the most surprising finding of our study is that, compared to theta oscillations, gamma oscillations in V4 remained less affected by the lesion in V1, which is at odds with the proposal of gamma as a feedforward signal [6,10,47]. What might then be the source of this V1-independent gamma in V4? One possibility is that it may reflect weak preserved gamma-rhythmic V1 input from the border of the lesion zone. While we cannot entirely rule out this scenario, it seems unlikely as it would involve an intact V1-V4 transmission circuit that cannot easily explain the > 100 ms delayed emergence of the gamma response with little change in amplitude. A similar interpretation of post-lesional gamma activity as a mere reflection of (non-rhythmic) residual MUA appears also unlikely: For one, under our testing conditions, there was no significant correlation between MUA and LFP gamma power before as well as after the V1 lesion. Whereas the lesion delayed MUA onset in V4 by <15 ms relative to prelesion conditions, LFP gamma power was delayed by > 100 ms after the lesion. Though it is tempting to compare residual V1 input to low-contrast stimulation conditions, the latency delay accounted for stimulation at low contrast [48–50] would only explain the delay in MUA, but not the more pronounced effect in the LFP. A third possibility, that this gamma oscillation is a result of microsaccades [51], also appears unlikely, given the narrowband frequency range of the oscillation and its sustained time course. A fourth possibility builds up on the thalamic, V1-bypassing inputs to V4, which can account for at least part of the residual activity in V4. Yet that gamma in V4 is inherited from direct LGN or Pulvinar input to V4 appears unlikely, again due to latency considerations and also as gamma has so far not been reported for these brain structures.

Irrespective of the actual source of the input source to V4 in our experiments, these inputs are able to induce sufficiently strong interactions between local excitatory and inhibitory networks within V4 to generate gamma. Our results thus hint at a very local origin of gamma oscillations within the microcircuit of an area. According to this view, a visual stimulus will drive a sweep of excitation across cortical areas that is associated with subsequent increases in gamma response in each area, simply due to the repeated gamma generating microarchitecture in each area. However secondary synchronization of local excitatory activity might be a very useful marker of ongoing interareal communication,

In this study, we tested the hypothesis that theta and gamma rhythms act as sensory feedforward signals from V1 to V4 when monkeys viewed a visual contour illusion. With intact cortex both oscillations were present in both areas, interacted in time and showed stronger illusory contour related activity in V4. While their predominant occurrence in V1 supragranular layers is consistent with a feedforward circuit, a direct causal test revealed a clear difference for the two rhythms: While lesioning V1 eliminated the theta rhythm of V4, gamma rhythms were less affected. This result supports the proposed function for feedforward processing from V1 to V4 of theta but not gamma rhythms and poses, together with the increasing literature body of the stimulus dependency of gamma [52–55], limits on the proposed role of gamma as a feedforward mechanism.

STAR Methods

RESOURCE AVAILABILITY

Lead Contact—Further information and requests for resources should be directed to and will be fulfilled by the Lead Contact, Ricardo Kienitz (ricardo.kienitz@esi-frankfurt.de).

Materials Availability—This study did not generate new unique items, such as animal lines or reagents.

Data and Code Availability—The data underlying the figures were deposited on a public repository (https://doi.org/10.12751/g-node.nb4nnp).

EXPERIMENTAL MODEL AND SUBJECT DETAILS

Two healthy adult female and two male rhesus monkeys (*Macaca mulatta*, monkey B, F, K and Br) were used in the study. All procedures were in accordance with the Institute for Laboratory Animal Research Guide for the Care and Use of Laboratory Animals and approved by the Animal Care and Use Committees of the National Institute of Mental Health and Vanderbilt University or by the Regierungspräsidium Darmstadt in accordance with EU directive 2010/63. All surgeries were carried out aseptically under general anesthesia using standard techniques including peri-surgical analgesia and monitoring. Each monkey received a head-immobilization implant and an implant to record neural data (see section below on Neurophysiology). Throughout the study animal welfare was monitored by veterinarians, technicians and scientists.

METHOD DETAILS

Parts of the dataset underlying this study (V4 data from monkey B and F) have been analysed and published with regard to the dependence of a Kanizsa-specific increase in single (and multi-) unit spiking on the receptive field focus [56]. The respective study did not study oscillatory signals.

Behavioral task and visual stimulation—Each monkey was trained to maintain fixation within a 1–1.5° diameter window centered on a small red spot (0.2° diameter, white for monkey K) during the presentation of various visual stimuli. To map receptive fields, white random dot kinematograms (1.5° diameter, see [56] for details) were shown on a black background at 64 different positions in the lower right visual hemifield. The Kanizsa illusion and the control stimulus consisted of four inducers (~1° diameter) located at (1°, −1°), (3°, −1°), (1°, −3°) and (3°, −3°), presented for 1 s (1.5 s in V1 recordings) after 1 s of fixation baseline. Each inducer consisted of a white disk with one quarter of the circle colored in red, giving them a “pacman-like” appearance. For the illusory stimulus, the red quarter faced the inner illusory surface (IF1 in [56]) creating an illusory rectangle. The control stimulus consisted of inducers that were rotated by 180° such that the red cutouts were facing outward (CF1 in [56]). For monkey K, the stimulus position was adapted to the V1 receptive fields (center of stimulus: x = 1°, y = −4.2°). V1 receptive field centers ranged from 0.06° to 4.7° and from −6.7° to −0.9° along the horizontal and vertical meridian respectively. For the laminar V1 recordings, the Kanizsa stimulus and its control were positioned such that the receptive field focus (RFF, see [56]) of the recording site was centered on the illusory parts of the stimulus.

Neurophysiology and chronic cortical lesioning—Neurophysiological data was recorded via chronically implanted multi-microelectrode (“Utah”) arrays that were located in area V4 (monkeys B and F) or V1 (monkey K) (see [19] for details regarding surgery and implantation). Each electrode was spaced 400 μm from its neighboring electrodes, and 1.5 mm (0.6 and 1.5 mm for monkey K) long. Neural data from monkeys B and F was recorded at a sampling rate of 24414.1 Hz using a Tucker Davis Technology system and at 30 kHz for monkeys K and Br on a Blackrock Microsystems Cerebus System. Following 13 sessions in monkey B and 6 sessions in monkey F, permanent focal aspiration lesions of isohemispheric primary visual cortex (V1) were performed (see [23] for details). After the lesion, post-lesion data were recorded in 15 and 6 sessions for monkey B and monkey F, respectively. To confirm the visual deficit (scotoma) following the V1 lesion, monkeys performed a perimetry task covering the lower right quadrant (see [20] for details). Data from monkey K was collected in two sessions. Layer-resolved V1 data was recorded from monkey Br using a linear microelectrode array, consisting of 22–24 active microelectrodes, linearly spaced 0.1 mm apart, with impedances ranging 0.2–0.8 MΩ at 1kHz (UProbe, Plexon). Electrical reference for data from the UProbe was the probe shaft.

QUANTIFICATION AND STATISTICAL ANALYSIS

Data preprocessing—All neurophysiological data were processed and analyzed using custom-written code for MATLAB (MathWorks, Inc.) and the FieldTrip MATLAB toolbox [57]. The continuous recordings were separated into individual stimulus presentations

(trials) using digital event markers aligned on stimulus onset. We focused our analyses on the sustained response period 300–1000 ms after stimulus onset, excluding the transient onset response. Trials containing motion artifacts were excluded by visual inspection without knowledge of trial type. Four dysfunctional recording channels in monkey B, four in monkey F and two in monkey K were excluded from the analysis. Details on receptive field mapping can be found in Cox et al., 2013. An estimate for multi-unit activity (MUA) was obtained from the high frequency envelope: MUA was extracted by high-pass filtering (300–12000 Hz), followed by rectification, and low-pass filtering (120 Hz) of the broadband data (see [19] for further details). The local field potential (LFP) was obtained by low-pass filtering the signal at 256 Hz. Data from microelectrode arrays was pooled across sessions. In order to assess the stimulus-specific effects of the Kanizsa illusion, data were normalized using the average baseline value (−0.7 – 0 s of prestimulus fixation period). MUA and powerspectra are expressed as percent change from this baseline.

Spectral analysis—To obtain the spectral profile of MUA and LFP responses, we used a Hanning-tapered Fourier transformation. Visual inspection of the spectra revealed peaks in the 3–6 Hz and 25–70 Hz bands (monkey B: 25–40, monkey F: 30–60 Hz, monkey K: 40–70 Hz), which are referred to as theta and (low) gamma, respectively. To obtain time-frequency representations (Figure 1), we performed a wavelet transform based on Morlets. To optimally assess low and high frequency components, we separately analyzed frequencies from 1–20 Hz (“low frequencies”, width 3 cycles, 1.3 Hz bandwidth at 4 Hz, 0.01 Hz steps) and >20 Hz (“high frequencies”, width 7 cycles, 15.7 Hz bandwidth at 40 Hz). As described above, analyses including spectral assessment focused on the sustained response period 300–1000 ms after stimulus onset.

Cross-frequency coupling—In order to assess phase-to-amplitude coupling between theta and gamma oscillations in the LFP, we computed a modulation index MI as follows [14]: The original LFP Signal $S(t)$ was bandpass-filtered into the theta and gamma ranges, respectively, using a two-pass filter (fourth order Butterworth) to avoid frequency-dependent phase shifts: $S_\theta(t)$ and $S_\gamma(t)$. As a next step, the Hilbert transform h of both signals was computed, producing complex values whose real components represent the amplitude of the signal and the imaginary part represent phase: $h(S_\theta(t))$ and $h(S_\gamma(t))$. From the Hilbert-transformed signals we extracted the phases of the theta signal $\Phi_{S_\theta}(t)$ and the amplitude from the gamma signal $A_{S_\gamma}(t)$. The composite signal $\left[\Phi_{S_\theta}(t), A_{S_\gamma}(t)\right]$ describes the amplitude of S_γ at each phase of S_θ. The phases $\Phi_{S_\theta}(t)$ were then binned ($n = 18$) and the mean amplitude $\left\langle A_{S_\gamma}\right\rangle(j)$ over each bin j was calculated and normalized by dividing by the sum of all bins, resulting in the normalized distribution-like function $P(j)$. Finally, the Modulation Index (MI) was defined as the normalized Kullback-Leibler divergence (KL) computed between $P(j)$ and a uniform distribution $Q(j)$ as follows:

$$D_{KL}(P,Q) = \sum_{j=1}^{n} P(j) log\, log\left(\frac{P(j)}{Q(j)}\right)$$

$$MI = \frac{D_{KL}}{log(n)}$$

We tested for significant modulation using a Monte Carlo technique, where we randomly permuted the amplitude-signal trial-wise against the phase-signal 500 times. To test for significant differences between Kanizsa illusion and control conditions, we performed a matched non-parametric test (Wilcoxon signed rank test) across channels. *MI* comes with several caveats (see [14] for a discussion). To avoid an overestimation of phase-amplitude coupling we verified that (1) there were clear peaks in the TFR and powerspectrum at the frequencies of interest (theta and gamma) and (2) that frequency band used for amplitude (gamma, 25–50 Hz) was at least double the frequency we used for the phase signal (theta, 3–6 Hz). To compute the Comodulogram (Figure 2A, middle panel) phase frequencies ranged from 5 to 10 Hz (±2 Hz) and amplitude frequencies from 15 to 80 Hz (±10 Hz). To compute the theta-phase triggered spectrogram (Figure 2A, right panel), the amplitude of bandpass-filtered high frequency (ranging from 10 to 80 Hz) was triggered on theta oscillation troughs and averaged across trials.

Analysis of laminar V1 data—To obtain a more localized measure of neural activity based on the LFP, and to locate electrodes on the U-Probe across cortical layers, we computed the laminar current source density (CSD) by approximating the second spatial derivative of the LFP [58]. The CSD constitutes a measure of localized current flow, which can be used to delineate upper from middle and lower cortical layers [17]. The transition from granular to infragranular layers was visually identified by selecting the bottom of the initial response sink of the CSD profile of the respective recording session [17]. We computed the laminar theta power based on MUA [43] and the laminar theta and gamma power based on LFP. The average laminar profiles were smoothed by fitting a spline for display purpose. Significance was assessed using a one-sided Wilcoxon signed rank test against baseline, $n = 9$).

Statistics—All statistical tests were done in MATLAB (MathWorks, Inc.) using their standard-implementation or custom-written code. Average values of the measures defined above (spectral power, PPC, MI) were calculated as the mean value across time and frequency. Differences between conditions were tested with nonparametric Wilcoxon signed rank tests (paired data) or to test if a distribution was significantly greater/smaller than zero, Mann-Whitney U tests (equals Wilcoxon rank sum test, unpaired data) or the computational resampling statistics described above. Data was smoothed for display purposes. To quantify effect sizes associated with the illusory stimulus, we computed the sensitivity measure

$$d' = \frac{\mu_K - \mu_C}{\sqrt{\frac{1}{2}\left(\sigma_K^2 + \sigma_C^2\right)}}$$

where μ_K and μ_C are the sample means and σ_K and σ_C the standard deviations for the Kanizsa and control conditions, respectively. To assess the strength of any residual theta rhythm (post lesion) we computed the signal-to-noise ratio:

$$SNR = 20\frac{\varphi\theta}{\varphi_n},$$

where φ_θ and φ_n are the power values in the theta (signal) and high frequency (noise) ranges (15–25 Hz (MUA) and 128–256 (LFP)), respectively. The percentage of variance explained was assessed by computing how well one signal predicted the other using a multilinear regression model. For the latency analysis (Figure 4I) we assessed the post-stimulus time point (excluding the initial transient, i.e. t >= 0.2 s) where gamma power significantly exceeded baseline levels on a channel-by-channel basis. Significance in this context was assessed using the Wilcoxon rank sum test for each post-stimulus time point across trials, followed by a Bonferroni-Holm correction. The time-point of reaching significance equaled the time-point where p-values within a sliding moving average window of 100 ms fell below alpha = 0.05 for the first time. Time points were then compared before and after the V1 lesion.

For the peak shift analysis (Figure 4J) pre- and post-lesional gamma peaks were defined as the strongest peak (as detected by the 'findpeaks' MATLAB function) in the gamma range after subtracting a fitted polynomial of degree 1 from the spectra (which allowed for better detection of smaller peaks) on a channel-by-channel basis. Gamma peaks were then compared before and after the V1 lesion.

Supplementary Material

Refer to Web version on PubMed Central for supplementary material.

Acknowledgments

This work was supported by an intramural NIH research grant to D.A.L. (ZIA-MH002838), a National Eye Institute Training Grant (2T32 EY007135-21) to K.D., an Alfred P. Sloan Fellowship, a Research Grant by the Whitehall Foundation and a Career Starter Grant by the Knights Templar Eye Foundation to A.M., a research grant from the National Eye Institute (1R01EY027402-02) to A.M. and M.C.S., Emmy Noether grant 2806/1 and ERC grant OptoVision 637638 to M.C.S..

References

1. Womelsdorf T, Fries P, Mitra PP, and Desimone R (2006). Gamma-band synchronization in visual cortex predicts speed of change detection. Nature 439, 733–736. [PubMed: 16372022]
2. Kienitz R, Schmiedt JT, Shapcott KA, Kouroupaki K, Saunders RC, and Schmid MC (2018). Theta Rhythmic Neuronal Activity and Reaction Times Arising from Cortical Receptive Field Interactions during Distributed Attention. Curr. Biol, 1–11.
3. Fiebelkorn IC, Saalmann YB, and Kastner S (2013). SI Rhythmic sampling within and between objects despite sustained attention at a cued location. Curr. Biol 23, 2553–8. [PubMed: 24316204]
4. Landau AN, and Fries P (2012). Attention samples stimuli rhythmically. Curr. Biol 22, 1000–4. [PubMed: 22633805]
5. Dugué L, Marque P, and VanRullen R (2015). Theta Oscillations Modulate Attentional Search Performance Periodically. J. Cogn. Neurosci 27, 945–58. [PubMed: 25390199]
6. Bastos AM, Vezoli J, Bosman CA, Schoffelen J-M, Oostenveld R, Dowdall JR, De Weerd P, Kennedy H, and Fries P (2015). Visual Areas Exert Feedforward and Feedback Influences through Distinct Frequency Channels. Neuron 85, 390–401. [PubMed: 25556836]

7. Spyropoulos G, Bosman CA, and Fries P (2018). A theta rhythm in macaque visual cortex and its attentional modulation. Proc. Natl. Acad. Sci 115, E5614–E5623. [PubMed: 29848632]
8. Bosman CA, Schoffelen J-M, Brunet N, Oostenveld R, Bastos AM, Womelsdorf T, Rubehn B, Stieglitz T, De Weerd P, and Fries P (2012). Attentional Stimulus Selection through Selective Synchronization between Monkey Visual Areas. Neuron 75, 875–88. [PubMed: 22958827]
9. Grothe I, Neitzel SD, Mandon S, and Kreiter a. K. (2012). Switching Neuronal Inputs by Differential Modulations of Gamma-Band Phase-Coherence. J. Neurosci. 32, 16172–16180. [PubMed: 23152601]
10. Kerkoerle T. van, Self MW, Dagnino B, Gariel-Mathis M-A, Poort J, van der Togt C, and Roelfsema PR (2014). Alpha and gamma oscillations characterize feedback and feedforward processing in monkey visual cortex. Proc. Natl. Acad. Sci 111, 14332–41. [PubMed: 25205811]
11. Burns SP, Xing D, and Shapley RM (2010). Comparisons of the dynamics of local field potential and multiunit activity signals in macaque visual cortex. J. Neurosci 30, 13739–13749. [PubMed: 20943914]
12. Nir Y, Fisch L, Mukamel R, Gelbard-Sagiv H, Arieli A, Fried I, and Malach R (2007). Coupling between Neuronal Firing Rate, Gamma LFP, and BOLD fMRI Is Related to Interneuronal Correlations. Curr. Biol 17, 1275–1285. [PubMed: 17686438]
13. Canolty RT, and Knight RT (2010). The functional role of cross-frequency coupling. Trends Cogn. Sci 14, 506–15. [PubMed: 20932795]
14. Aru JJ, Aru JJ, Priesemann V, Wibral M, Lana L, Pipa G, Singer W, and Vicente R (2015). Untangling cross-frequency coupling in neuroscience. Curr. Opin. Neurobiol 31, 51–61. [PubMed: 25212583]
15. Felleman DJ, and Van Essen DC (1991). Distributed hierarchical processing in the primate cerebral cortex. Cereb. Cortex 1, 1–47. [PubMed: 1822724]
16. Markov NT, Vezoli J, Chameau P, Falchier A, Quilodran R, Huissoud C, Lamy C, Misery P, Giroud P, Ullman S, et al. (2014). Anatomy of hierarchy: Feedforward and feedback pathways in macaque visual cortex. J. Comp. Neurol 522, 225–259. [PubMed: 23983048]
17. Maier A, Aura CJ, and Leopold D a (2011). Infragranular sources of sustained local field potential responses in macaque primary visual cortex. J. Neurosci 31, 1971–1980. [PubMed: 21307235]
18. Maier A, Adams GK, Aura C, and Leopold D. a (2010). Distinct superficial and deep laminar domains of activity in the visual cortex during rest and stimulation. Front. Syst. Neurosci 4, 1–11. [PubMed: 20204156]
19. Schmid MC, Schmiedt JT, Peters AJ, Saunders RC, Maier A, and Leopold D. a (2013). Motion-sensitive responses in visual area V4 in the absence of primary visual cortex. J. Neurosci 33, 18740–5. [PubMed: 24285880]
20. Schmiedt JT, Maier A, Fries P, Saunders RC, Leopold D. a, and Schmid MC (2014). Beta oscillation dynamics in extrastriate cortex after removal of primary visual cortex. J. Neurosci 34, 11857–64. [PubMed: 25164679]
21. Rodman HR, Sorenson KM, Shim AJ, and Hexter DP (2001). Calbindin immunoreactivity in the geniculo-extrastriate system of the macaque: Implications for heterogeneity in the koniocellular pathway and recovery from cortical damage. J. Comp. Neurol 431, 168–181. [PubMed: 11169998]
22. Fries W (1981). The projection from the lateral geniculate nucleus to the prestriate cortex of the macaque monkey. Proc. R. Soc. London. Ser. B, Biol. Sci 213, 73–86. [PubMed: 6117869]
23. Schmid MC, Mrowka SW, Turchi J, Saunders RC, Wilke M, Peters AJ, Ye FQ, and Leopold D. a (2010). Blindsight depends on the lateral geniculate nucleus. Nature 466, 373–7. [PubMed: 20574422]
24. Alexander GE, and Fuster JM (1973). Firing Changes in Cells of the Nucleus Medialis Dorsalis associated with delayed Response Behavior. Brain Res 61, 79–91. [PubMed: 4204130]
25. Ramcharan EJ, Gnadt JW, and Sherman SM (2005). Higher-order thalamic relays burst more than first-order relays. Proc. Natl. Acad. Sci. U. S. A 102, 12236–12241. [PubMed: 16099832]
26. Hall TM, de Carvalho F, and Jackson A (2014). A common structure underlies low-frequency cortical dynamics in movement, sleep, and sedation. Neuron 83, 1185–1199. [PubMed: 25132467]
27. Susilaradeya D, Xu W, Hall TM, Galán F, Alter K, and Jackson A (2019). Extrinsic and intrinsic dynamics in movement intermittency. Elife 8.

28. Jutras MJ, Fries P, and Buffalo E a (2013). Oscillatory activity in the monkey hippocampus during visual exploration and memory formation. Proc. Natl. Acad. Sci 110, 13144–13149. [PubMed: 23878251]
29. Lakatos P, Shah AS, Knuth KH, Ulbert I, Karmos G, and Schroeder CE (2005). An oscillatory hierarchy controlling neuronal excitability and stimulus processing in the auditory cortex. J. Neurophysiol 94, 1904–1911. [PubMed: 15901760]
30. Wilke M, Logothetis NK, and Leopold D. a(2006). Local field potential reflects perceptual suppression in monkey visual cortex. Proc. Natl. Acad. Sci. U. S. A 103, 17507–12. [PubMed: 17088545]
31. Lee H, Simpson GV, Logothetis NK, and Rainer G (2005). Phase locking of single neuron activity to theta oscillations during working memory in monkey extrastriate visual cortex. Neuron 45, 147–56. [PubMed: 15629709]
32. Liebe S, Hoerzer GM, Logothetis NK, and Rainer G (2012). Theta coupling between V4 and prefrontal cortex predicts visual short-term memory performance. Nat. Neurosci 15, 456–62, S1–2. [PubMed: 22286175]
33. Sheinberg DL, and Logothetis NK (1997). The role of temporal cortical areas in perceptual organization. Proc. Natl. Acad. Sci. U. S. A 94, 3408–3413. [PubMed: 9096407]
34. Rollenhagen JE, and Olson CR (2005). Low-frequency oscillations arising from competitive interactions between visual stimuli in macaque inferotemporal cortex. J. Neurophysiol 94, 3368–87. [PubMed: 15928064]
35. Raghavachari S, Kahana MJ, Rizzuto DS, Caplan JB, Kirschen MP, Bourgeois B, Madsen JR, and Lisman JE (2001). Gating of human theta oscillations by a working memory task. J. Neurosci 21, 3175–3183. [PubMed: 11312302]
36. Siapas AG, Lubenov EV, and Wilson M. a (2005). Prefrontal phase locking to hippocampal theta oscillations. Neuron 46, 141–51. [PubMed: 15820700]
37. Schmid MC, and Maier A (2015). To see or not to see – Thalamo-cortical networks during blindsight and perceptual suppression. Prog. Neurobiol
38. Lisman JE, and Jensen O (2013). The Theta-Gamma neural code. Neuron 77, 1002–16. [PubMed: 23522038]
39. Buzsáki G, and Wang X-J (2012). Mechanisms of gamma oscillations. Annu. Rev. Neurosci 35, 203–25. [PubMed: 22443509]
40. von Stein a, Chiang C, and König P (2000). Top-down processing mediated by interareal synchronization. Proc. Natl. Acad. Sci. U. S. A 97, 14748–14753. [PubMed: 11121074]
41. Rockland KS, and Pandya DN (1979). Laminar origins and terminations of cortical connections of the occipital lobe in the rhesus monekey. Brain Res
42. Rauch A, Rainer G, and Logothetis NK (2008). The effect of a serotonin-induced dissociation between spiking and perisynaptic activity on BOLD functional MRI. Proc. Natl. Acad. Sci. U. S. A 105, 6759–6764. [PubMed: 18456837]
43. Kajikawa Y, and Schroeder CE (2011). How local is the local field potential? Neuron 72, 847–858. [PubMed: 22153379]
44. Otero-Millan J, Troncoso XG, Macknik SL, Serrano-Pedraza I, and Martinez-Conde S (2008). Saccades and microsaccades during visual fixation, exploration, and search: foundations for a common saccadic generator. J. Vis 8, 21.1–18.
45. Chota S, Luo C, Crouzet SM, Boyer L, Kienitz R, Schmid MC, and Vanrullen R (2018). Rhythmic fluctuations of saccadic reaction time arising from visual competition. Sci. Rep 8, 1–7. [PubMed: 29311619]
46. Landau AN, Schreyer HM, van Pelt S, and Fries P (2015). Distributed Attention Is Implemented through Theta-Rhythmic Gamma Modulation. Curr. Biol 25, 2332–2337. [PubMed: 26279231]
47. Self MW, van Kerkoerle T, Supèr H, and Roelfsema PR (2013). Distinct Roles of the Cortical Layers of Area V1 in Figure-Ground Segregation. Curr. Biol, 2121–2129. [PubMed: 24139742]
48. Reich DS, Mechler F, and Victor JD (2001). Temporal coding of contrast in primary visual cortex: When, what, and why. J. Neurophysiol 85, 1039–1050. [PubMed: 11247974]
49. Gawne TJ (2000). The simultaneous coding of orientation and contrast in the responses of V1 complex cells. Exp. Brain Res 133, 293–302. [PubMed: 10958519]

50. Sundberg KA, Mitchell JF, Gawne TJ, and Reynolds JH (2012). Attention influences single unit and local field potential response latencies in visual cortical area V4. J. Neurosci 32, 16040–16050. [PubMed: 23136440]
51. Yuval-Greenberg S, Tomer O, Keren AS, Nelken I, and Deouell LY (2008). Transient Induced Gamma-Band Response in EEG as a Manifestation of Miniature Saccades. Neuron 58, 429–441. [PubMed: 18466752]
52. Eleonora Bartoli A, Bosking W, Chen Y, Beauchamp MS, Yoshor D, Bartoli E, Li Y, Sheth SA, and Foster BL (2019). Functionally Distinct Gamma Range Activity Revealed by Stimulus Tuning in Human Visual Cortex Article Functionally Distinct Gamma Range Activity Revealed by Stimulus Tuning in Human Visual Cortex. Curr. Biol 29, 3345–3358. [PubMed: 31588003]
53. Gray CM, and Singer W (1989). Stimulus-specific neuronal oscillations in orientation columns of cat visual cortex. Proc. Natl. Acad. Sci. U. S. A 86, 1698–702. [PubMed: 2922407]
54. Gieselmann MA, and Thiele A (2008). Comparison of spatial integration and surround suppression characteristics in spiking activity and the local field potential in macaque V1. Eur. J. Neurosci 28, 447–459. [PubMed: 18702717]
55. Peter A, Uran C, Klon-Lipok J, Roese R, Van Stijn S, Barnes W, Dowdall JR, Singer W, Fries P, and Vinck M (2019). Surface color and predictability determine contextual modulation of V1 firing and gamma oscillations. Elife 8, 1–38.
56. Cox M. a, Schmid MC, Peters AJ, Saunders RC, Leopold D. a, and Maier A (2013). Receptive field focus of visual area V4 neurons determines responses to illusory surfaces. Proc. Natl. Acad. Sci. U. S. A 110, 17095–100. [PubMed: 24085849]
57. Oostenveld R, Fries P, Maris E, and Schoffelen J-M (2011). FieldTrip: Open source software for advanced analysis of MEG, EEG, and invasive electrophysiological data. Comput. Intell. Neurosci
58. Mitzdorf U (1985). Current source-density method and application in cat cerebral cortex: investigation of evoked potentials and EEG phenomena. Physiol. Rev 65, 37–100. [PubMed: 3880898]

Highlights

- Visual stimulation elicits theta and gamma oscillations in V1 and V4
- Theta and gamma oscillations interact in time
- While lesion of V1 eliminates V4 theta oscillations, gamma oscillations survive
- Gamma oscillations still contain stimulus information but emerge delayed without V1

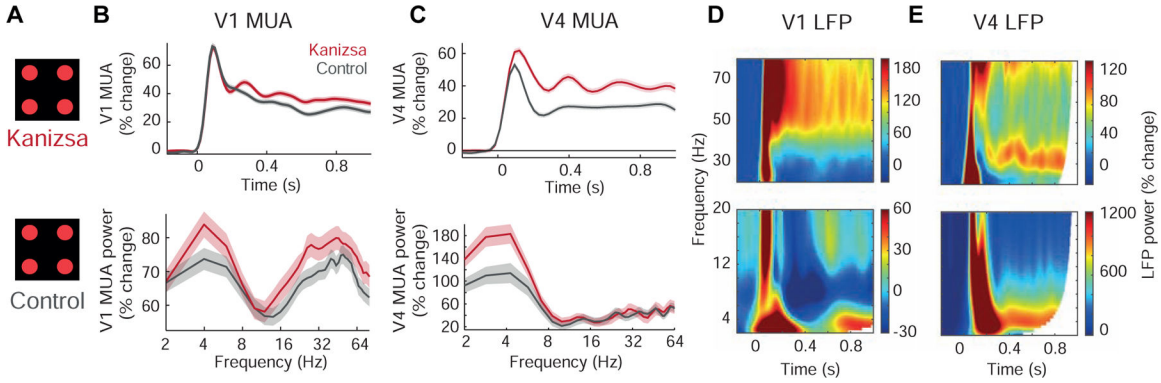

Figure 1. Rhythmic theta activity in V1 and V4 in response to the Kanizsa illusion.

(A) Depiction of the Kanizsa illusion (upper panel) and the control stimulus (lower panel).

(B) Upper panel: example V1 MUA response from one representative electrode channel; lower panel: MUA powerspectrum for area V1 averaged across channels from monkey K. Kanizsa (red) and control conditions (gray), shaded areas depict SEM.

(C) Same as **(B)** but for V4 (monkey B).

(D) Time-frequency representations of V1 LFP, averaged across channels from monkey K for the Kanizsa condition for low (lower panel) and high frequencies (top panel). Low and high frequencies are displayed separately due to the large increase in the theta range.

(E) Same as **(D)** but V4 (monkey B).

See also Figure S1 Table S1–3.

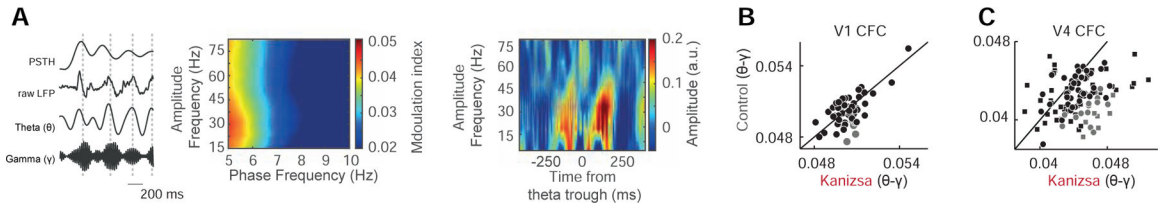

Figure 2. Theta-phase-to-gamma-amplitude coupling in V1 and V4.

(A) Left panel, from top: MUA response of one example electrode channel (averaged across trials), raw LFP, as well as theta and gamma band-pass filtered extracellular voltages for the ~ −0.1–1 s trial period (monkey B, Kanizsa condition). Vertical dashed lines highlight the temporal relationship between highest gamma amplitudes to both theta LFP and theta-modulated MUA. Axes are rescaled for display purposes. Middle panel: Comodulgram for Modulation Indices (MI) averaged across V4 channels from monkey B for the Kanizsa illusion. Right panel: theta-phase triggered spectrum from one example channel from monkey B.

(B) Scatter plot showing the distribution of MI as a measure for phase-to-amplitude coupling for significantly modulated V1 electrode channels for the Kanizsa vs. control conditions from monkey K. Average MI values were not significantly higher for the Kanizsa compared to the control stimulus ($p = 0.055$, n = 61, Wilcoxon paired signed rank test). Gray color highlights channels that showed significantly higher MI for the Kanizsa illusion compared to the control.

(C) Same as **(B)** but for V4 LFP from monkey B (circles) and F (squares) for the Kanizsa vs. control conditions. Average MI values were significantly higher for the Kanizsa compared to the control stimulus ($p = 7.7 \times 10^{-9}$, n = 60 in monkey B, $p = 2.2 \times 10^{-5}$, n = 50 in monkey F, Wilcoxon paired signed rank test).

See also Table S4.

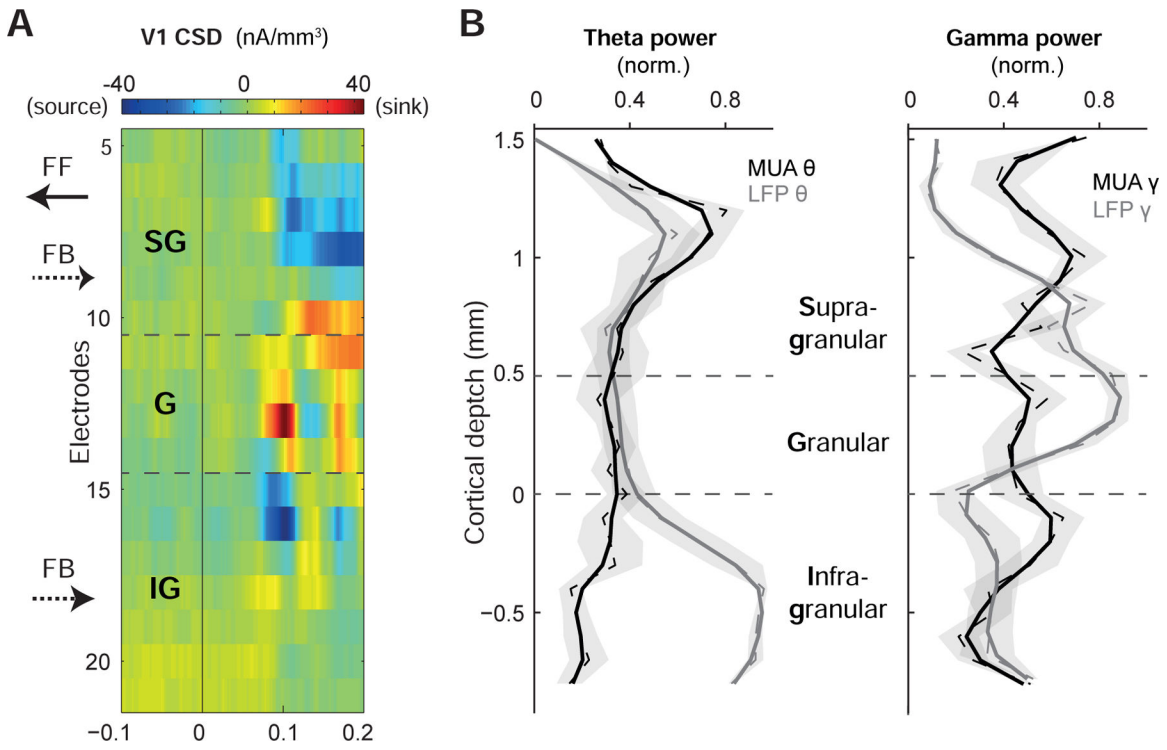

Figure 3. Laminar distribution of theta and gamma activity in V1.

(A) Current source density (CSD) based on the layer-resolved LFP of a linear multi-contact electrode for one example session representing the laminar profile of visually evoked responses in V1. FF: feedforward, FB: feedback to and from V4, SG: supragranular, IG: infragranular.

(B) Left panel: average and normalized V1 MUA (black) and LFP (gray) theta power (n = 9 sessions) as a function of cortical depth. Raw data is shown as dashed, smoothed data as solid lines, shaded areas depict SEM. Right panel: same as left panel, but for V1 MUA (black) and LFP (gray) gamma power.

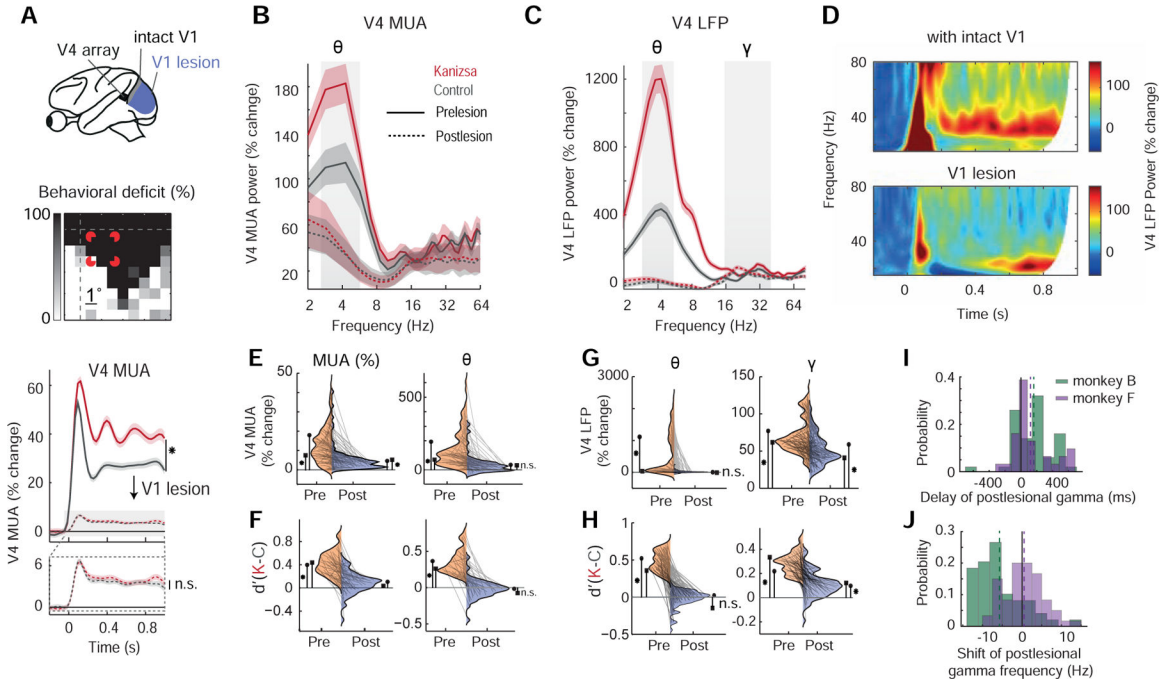

Figure 4. Effect of V1 lesion on rhythmic neuronal activity in V4.

(A) Diagram indicating the extent of the focal V1 aspiration lesion (top panel). Middle panel shows the visual deficit of monkey B in a spatial detection task following the lesion (lower right quadrant); note that this scotoma covered the Kanizsa stimulus (in red for display purpose) approximately by half. Lower panel depicts V4 MUA response from one example electrode channel from monkey B before (solid lines) and after the focal V1 lesion (dashed lines) for the Kanizsa illusion (red) and control condition (gray). Postlesional activity is shown (rescaled) in lower magnified panel. Shaded areas depict SEM.

(B) MUA powerspectrum averaged across channels from monkey B for Kanizsa illusion (red) and control condition (gray) pre- (solid lines) and postlesion (dashed lines), showing the elimination of theta activity. Shaded areas depict SEM

(C) Same as **(B)**, but LFP powerspectrum averaged across channels from monkey B. Note the preservation of activity in the gamma range despite the elimination of theta oscillations.

(D) Time-frequency representations of one example V4 electrode channel form monkey B depicting high LFP frequencies before (upper panel) and after the focal V1 lesion (lower panel).

(E) Distributions of MUA (left panel) and theta modulation of MUA (right panel) before (orange, left wings) and after the V1 lesion (blue, right wings) for the Kanizsa illusion. Individual pairs represent individual channels (data averaged across trials) and are shown for monkey B and monkey F, lateral symbols depict means (circle for monkey B, square for monkey F). Asterisks denote significance relative to zero (n.s. = non-significant) and refer to consistent results for both monkeys.

(F) Same as **(E)** but for d' values (Kanizsa illusion vs. control) based on MUA (left panel) and theta modulation of MUA (right panel).

(G) Distributions of LFP theta (left panel) and gamma power changes (right panel) before (orange, left wings) and after the V1 lesion (blue, right wings) for the Kanizsa illusion.

Individual connected data pairs represent individual channels (data averaged across trials) and are shown for monkey B and monkey F, lateral symbols depict means (circle for monkey B, square for monkey F). Asterisks denote significance relative to zero (n.s. = non-significant) and refer to consistent results for both monkeys.

(H) Same as **(G)** but for d' values (Kanizsa illusion vs. control) based on LFP theta (left) and gamma power (right). Note that, while theta activity lost its Kanizsa-association, gamma responses maintained information about the Kanizsa stimulus even without V1.

(I) Histogram showing the distribution of the postlesional gamma delay across LFP channels for monkey B (green) and F (purple). Positive values indicate a later onset of gamma power after the V1 lesion. Vertical dashed lines highlight mean values for both monkeys.

(J) Histogram showing the distribution of postlesional shift in peak gamma frequency across LFP channels for monkey B (green) and F (purple). Positive values indicate an increase of the peak gamma frequency after the V1 lesion. Vertical dashed lines highlight mean values for both monkeys.

See also Figure S2 and Table S5.

Table 1:

Recordings performed in individual monkeys.

Recordings / Monkey	Monkey B	Monkey F	Monkey K	Monkey Br
V4 Utah-Array before and after V1 lesion	X	X		
V1 Utah-Array			X	
V1 linear U-Probe				X

KEY RESOURCES TABLE

REAGENT or RESOURCE	SOURCE	IDENTIFIER
Antibodies		
Bacterial and Virus Strains		
Biological Samples		
Chemicals, Peptides, and Recombinant Proteins		
Critical Commercial Assays		
Deposited Data		
Data underlying the figures		https://doi.org/10.12751/g-node.nb4nnp
Experimental Models: Cell Lines		

REAGENT or RESOURCE	SOURCE	IDENTIFIER
Experimental Models: Organisms/Strains		
Macaca mulatta	Public Health England, Porton Down, UK	Monkey K
Macaca mulatta	Wake Forest University (Winston-Salem, North Carolina)	Monkey Br
Macaca mulatta	NIH Primate Services, Poolesville, USA	Monkey B Monkey F
Oligonucleotides		
Recombinant DNA		
Software and Algorithms		
MATLAB	The MathWorks	https://www.mathworks.com/products/matlab.html
Fieldtrip toolbox	[57]	http://www.fieldtriptoolbox.org/
Other		
Infrared video eye tracking system	EyeLink	https://www.sr-research.com
Data Acquisition System	Blackrock Microsystems	http://blackrockmicro.com
Data Acquisition System	Tucker Davis Technology system	https://www.tdt.com
Data Acquisition System	Plexon, UProbe	https://plexon.com